Improvement of the study of heat sink dynamics in elastocaloric materials by Gaussian filtering

Author: Guillem Capellera Font
*Facultat de Física, Universitat de Barcelona, Diagonal 645, 08028 Barcelona, Spain.**

Advisors: Eduard Vives Santa-Eulalia
(Dated: June 22, 2021)

Abstract: In this work we study the cooling process that occurs in a metal sample when it experiences a structural phase transition during a stress release. A previous study using an infrared (IR) camera determined the temperature map evolution of the sample surface. Reversing the Fourier heat equation allows to find the heat sinks, where cooling associated with latent heat exchange occurs. We reanalyze the data of the previous study and we improve the results by a numerical analysis based on a Gaussian filter. Indeed, the results show a better location of the heat sinks, which has made possible to properly determine its size, magnitude and velocity.

I. INTRODUCTION

Shape memory alloys [1] are metals that exhibit several interesting thermomechanical properties such as elastocaloric effects and superelasticity [2]. Some of these properties can be used to design solid state environmentally friendly "cooling" devices that will avoid the use of greenhouse effect gases [3, 4].

When these compounds are subject to an external stress or a change in temperature, their microstructure shows a first-order phase transition from a high symmetry cubic phase to a lower symmetry martensitic phase [5]. This is the so-called thermoelastic martensitic transformation (MT). As occurs with first-order phase transitions it exhibits a latent heat exchange and it is reversible but with hysteresis.

The transition takes place through nucleation and domain growth which create fronts that advance in a non-homogeneous and discontinuous manner along the samples [6]. When the transition takes place in the direction from martensite to cubic (decreasing stress or increasing temperature) the fronts advance absorbing energy from the material and consequently cooling it. In the reverse direction from cubic to martensite, the fronts emit energy and locally heat the sample. Thus the fronts can be regarded as heat sinks or heat sources depending on the direction in which the transition takes place. One of the main challenges, at present, is to study the temporal and spatial behaviour of these heat sinks and sources.

The breakthrough of affordable infrared (IR) cameras has led to an increase in the number of thermal field analysis on sample surfaces during mechanical testing. IR imaging is a very useful technique for measuring temperature as a function of time and position, $T(\vec{r}, t)$ allowing to determine the evolution of non-homogeneous temperature distribution of the samples. Specifically, IR cameras are used to study the elastocaloric behaviour of different compounds. However, IR imaging does not directly reveal the location of heat sinks and heat sources. For this reason, data processing is performed in order to reverse the Fourier equation and visualize the fronts from the thermal maps [7]. Neglecting heat losses towards the air, the Fourier equation [8] can be expressed as:

$$\Sigma(\vec{r}, t) = \frac{\partial T(\vec{r}, t)}{\partial t} - \frac{\kappa}{C\rho}\Delta T(\vec{r}, t) \tag{1}$$

where C is the specific heat, ρ is the density, κ is the thermal conductivity and Σ is the power source/sink density.

The influence of experimental noise is a key issue to determine heat sinks and heat sources. The martensitic fronts moving through the sample are expected to have a well-defined location (sharp), so filtering should clear the external noise (white noise type) without distorting the spatial high frequencies associated with sharp fronts. The problem with filters based on uniform averaging is that they also remove high frequencies, so the front edges become more smooth. Contrarily, Gaussian filtering can be used as a filter that removes low frequencies associated with experimental noise but keeps high frequencies components associated with front edges [9].

This work is based on previous IR experiments where a uniform filter was used. We have repeated the data treatment using Gauss filtering and explored the range of parameters of the numerical processing in order to obtain a more accurate location of the heat sinks. This has allowed us to discover new physics that with the previous uniform filtering was impossible.

II. PREVIOUS INFRARED STUDY

In a previous experiment [10] a Cu-Al-Ni elastocaloric sample was studied. The sample was a cylindrical single crystal wire. The experiment consisted in the IR imaging during the unloading of the wire that was previously stressed, corresponding to the martensitic to cubic transition that involves the formation of heat sinks. The wire

*Electronic address: gcapelfo7@alumnes.ub.edu

was produced at Nimesis Technology and has a nominal composition of $Cu_{70.6\%}Al_{25.7\%}Ni_{3.7\%}$ atomic percent. The sample dimensions were 1 mm diameter and $\sim$ 30 mm length.

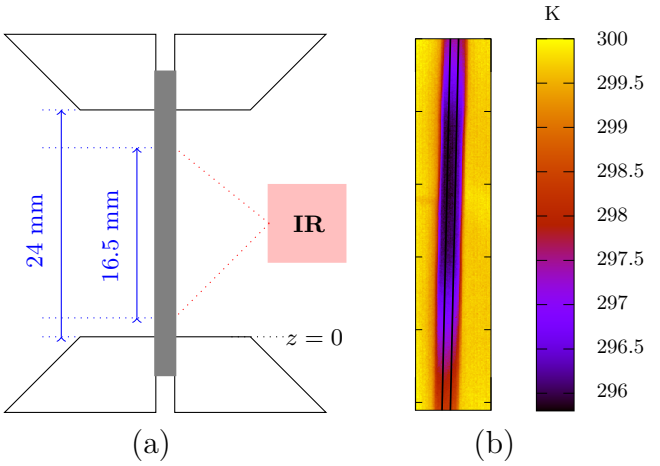

FIG. 1: (a) Schematic representation of the previous study, indicating the sample dimensions and the position of the IR imaged zone. (b) IR image corresponding to $t = 52$ s (frame 1870). The colour scale on the right corresponds to the temperatures. The observed black lines show the central zone of the wire (11 pixels for each horizontal line). These lines are slightly inclined due to the tilted orientation of the IR camera.

A Zwick/Roell Z005 testing machine was used to grip and stress the wire. Fig.1(a) illustrates a schematic representation of the test. The initial length of the sample between grips was $L = 24$ mm. Room temperature was $T_0 \simeq 299$ K. First, a loading stage was performed during 23.3 s at a speed of 0.1 mm/s until reaching an elongation of 2.3 mm. This was followed by a 10 s pause for the equilibration of the sample temperature with the environment. After, the unloading stage was performed at the same speed until reaching the initial elongation.

During unloading, two-dimensional temperature maps were obtained using an infrared thermographic camera (InfraTec 8300), as illustrated in Fig.1(a). The spatial resolution of the camera was 0.03226 mm/pixel, the temporal resolution was 0.01 s/frame and the temperature resolution was 1 mK. Once the data was obtained, a first numerical smoothing was performed to eliminate erroneous pixels with non-reasonable values. These values were replaced by the uniform average over the neighbouring pixels. Fig.1(b) illustrates an example of the images obtained corresponding to $t = 52$ s.

Since the camera was not exactly aligned and the wire was cylindrical, another numerical processing was performed in order to obtain the evolution of 1D thermal profile. For each horizontal line in the image, 11 pixels corresponding to the center of the sample were uniformly averaged. These pixels are found between the slightly inclined black lines represented in Fig.1(b).

Vertical profiles $T(i,k)$ were indexed with i (from 1 to 512) representing the vertical pixels and k (from 1 to 2230) representing the frames. Fig.2 shows the evolution of the thermal profile, revealing the temperature decrease in the central part of the sample.

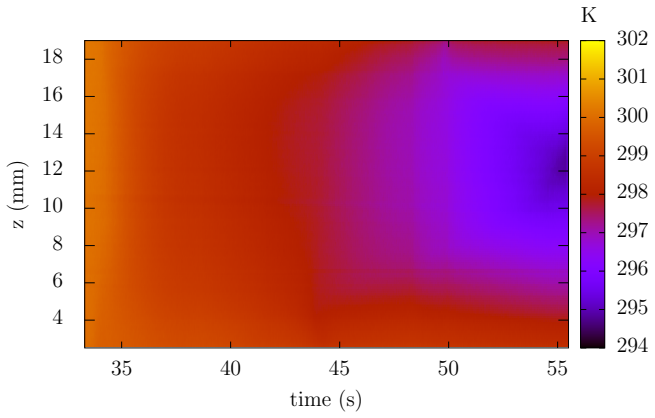

FIG. 2: Evolution of the vertical temperature profile as a function of time. The data corresponds to the unloading of the sample.

To obtain the dynamics and the location of the power sink density from the vertical temperature profiles, a numerical post-processing was performed using the Fourier equation (1) in its 1D form. The spatial coordinate z was replaced by $i \cdot \Delta z$ and the temporal coordinate t by $k \cdot \Delta t$:

$$\Sigma(i,k) = \frac{1}{\Delta t}\frac{\partial T(i,k)}{\partial k} - \frac{\kappa}{C\rho\Delta z^2}\frac{\partial^2 T(i,k)}{\partial i^2} \qquad (2)$$

Note that Σ is measured in Ks^{-1} and by multiplying it by $C\rho$ one would obtain the power sink density in Wm^{-3}. The first order time derivative refers to changes of temperature per frame and the second order space derivative refers to second order changes of temperature per square pixel.

In the previous work [10], in order to suppress the noise, a first step of the numerical post-processing consisted in performing a temporal and spatial smoothing of the vertical temperature profiles $T(i,k)$. To do so, for each pixel i, a uniform averaging over 5 frames (from $k-2$ to $k+2$) was performed in order to obtain the temporal smoothed profile $\bar{T}_A(i,k)$ (see eq. 3a). Then, for each frame k, another uniform averaging over 101 pixels (from $i-50$ to $i+50$) was performed in order to obtain the temporal and spatial smoothed profile $\bar{\bar{T}}_A(i,k)$ (see eq. 3b).

$$\bar{T}_A(i,k) = \frac{1}{5}\sum_{n=-2}^{2} T(i,k+n) \qquad (3a)$$

$$\bar{\bar{T}}_A(i,k) = \frac{1}{101}\sum_{n=-50}^{50} \bar{T}_A(i+n,k) \qquad (3b)$$

The second numerical step consisted in computing the first temporal and second spatial derivatives using the five-point stencil method (4) with increments of 20 frames and 30 pixels, respectively [11]:

$$\frac{\partial \bar{\bar{T}}_A(i,k)}{\partial k} \approx \frac{1}{12\cdot 20}\Big[-\bar{\bar{T}}_A(i,k+40)+8\bar{\bar{T}}_A(i,k+20)- \\ -8\bar{\bar{T}}_A(i,k-20)+\bar{\bar{T}}_A(i,k-40)\Big] \tag{4a}$$

$$\frac{\partial^2 \bar{\bar{T}}_A(i,k)}{\partial i^2} \approx \frac{1}{12\cdot 30^2}\Big[-\bar{\bar{T}}_A(i+60,k)+16\bar{\bar{T}}_A(i+30,k)- \\ -30\bar{\bar{T}}_A(i,k)+16\bar{\bar{T}}_A(i-30,k)- \\ -\bar{\bar{T}}_A(i-60,k)\Big] \tag{4b}$$

Finally, using the parameters represented on Table I, the spatial and temporal dependence of Σ was computed. Results are shown in Fig.3(a).

The authors concluded that a first front (lower front) advances from bottom to top of the sample and then, a second front (upper front) begins to advance from top to bottom. Finally the two fronts merge near the center of the sample producing a strong heat absorption at this point. However, it was difficult to obtain more quantitative results describing the physics of the fronts.

ρ [gcm^3]	7.12
C [JK^{-1}g^{-1}]	0.45
κ [Wm^{-1}K^{-1}]	45

TABLE I: Cu-Al-Ni parameters in the Fourier equation (2).

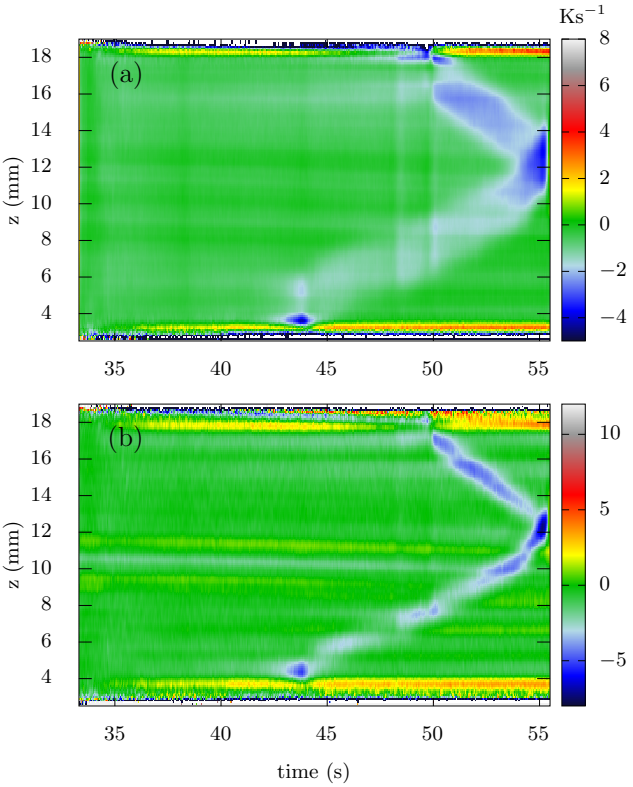

FIG. 3: Power sink density (in Ks^{-1}) as a function of time and position. Power sink density has been computed using vertical temperature profiles smoothed by (a) uniform averaging and (b) Gaussian filtering. Note that the colour scales are not the same between (a) and (b).

III. GAUSSIAN FILTERING

In the present work, the first step of the numerical post-processing has been modified. Gaussian filtering has been used, instead of uniform averaging, to obtain new smoothed vertical profile temperatures, $\bar{\bar{T}}_G(i,k)$.

We define the vector $G(N,\sigma)$ whose components are:

$$G_n(N,\sigma) = \frac{1}{\sqrt{2\pi\sigma^2}} e^{-\frac{n^2}{2\sigma^2}} \tag{5}$$

where $n = -N, ..., 0, ..., N$ is the index that corresponds to each component, and σ is the standard deviation of the Gaussian distribution. The N parameter refers to the width of the filter (in pixels or frames). It has been introduced to truncate the vector and consequently to get a finite impulse response. A tolerance ϵ has also been defined in order to ignore the components $G_n(N,\sigma)$ with values smaller than ϵ. Thus, the standard deviation σ depends on the width of the filter N and the tolerance ϵ. This function $\sigma(N,\epsilon)$ cannot be given explicitly, but implicitly as follows:

$$\epsilon = \frac{1}{\sqrt{2\pi\sigma^2(N,\epsilon)}} e^{-\frac{N^2}{2\sigma^2(N,\epsilon)}} \tag{6}$$

A mathematical software (*Wolfram Alpha*) has been used to solve this equation in order to find $\sigma(N,\epsilon)$ values.

This vector, $G(N,\sigma)$, has been applied to convolute the profiles $T(i,k)$ in order to obtain the temporal and spatial smoothed profiles. Following the same order as the previous study [10], we have performed the convolution for the time domain in order to obtain the temporal smoothed profile $\bar{T}_G(i,k)$ (see eq. 7a), and then for the spatial domain to obtain the temporal and spatial smoothed profile $\bar{\bar{T}}_G(i,k)$ (see eq. 7b). We have defined for each of the convolutions the widths of the filters as N_k frames and N_i pixels, respectively. The same tolerance $\epsilon = 10^{-5}$ has been considered in both domains.

$$\bar{T}_G(i,k) = \sum_{n=-N_k}^{N_k} T(i,k+n)\, G_n(N_k,\sigma(N_k,\epsilon)) \tag{7a}$$

$$\bar{\bar{T}}_G(i,k) = \sum_{n=-N_i}^{N_i} \bar{T}_G(i+n,k)\, G_n(N_i,\sigma(N_i,\epsilon)) \tag{7b}$$

For the temporal domain, the same width as the previous study has been used, $N_k = 2$. In order to find the optimal width for the spatial domain, a number of widths $N_i = 5, 10, 25, 50, 75, 100$ have been considered. For each one, Σ has been computed using the five-point stencil method, indicated in equation (4), in the same way as the second post-numerical step of the previous study. As an example, the obtained Σ values have been plotted for $t = 52$ s (frame 1870) in Fig.4. The criterion followed to choose the optimal width N_i is to maximize noise reduction but without losing definition of the edge fronts. By visualizing the graph, this means choosing the maximum value of N_i that still keeps a reasonable definition of the width of the fronts. According to the results, this corresponds to $N_i = 25$ pixels. Finally, the evolution of Σ with the chosen optimal parameters, has been represented in Fig.3(b).

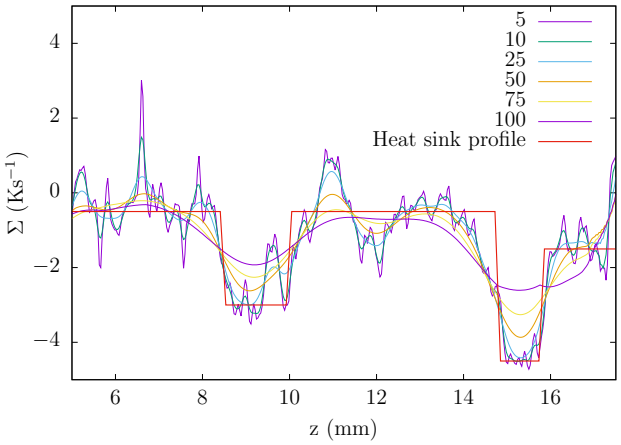

FIG. 4: Power sink density at $t = 52$ s as a function of position. Power sink density has been computed using vertical temperature profiles smoothed by Gaussian filtering with different widths $N_i = 5, 10, 25, 50, 75, 100$. Heat sink theoretical profile has been drawn (red colour) assuming that only two fronts exist (upper and lower) in order to choose the optimal width.

IV. RESULTS

The Gaussian filtering has made it possible to obtain a map of the evolution of the Σ distributions with a better definition of the fronts when compared to previous work [10]. Indeed, Fig.3(b) shows narrower fronts with greater magnitudes than the fronts in Fig.3(a) [10]. As can be seen in Fig.4, the lower front has a width of ~ 1.5 mm and the upper front a width of ~ 1 mm.

The first question to discuss is about the magnitude of the heat sink, Σ. Fig.3(a) reveals only small changes of heat sink magnitude during the propagation of each front. In contrast, Fig.3(b) shows that variations in the magnitude are more relevant.

The second question is that Fig.3(b) reveals sudden changes in the position of the fronts. These changes were more difficult to detect in Fig.3(a) because the width of the fronts was greater.

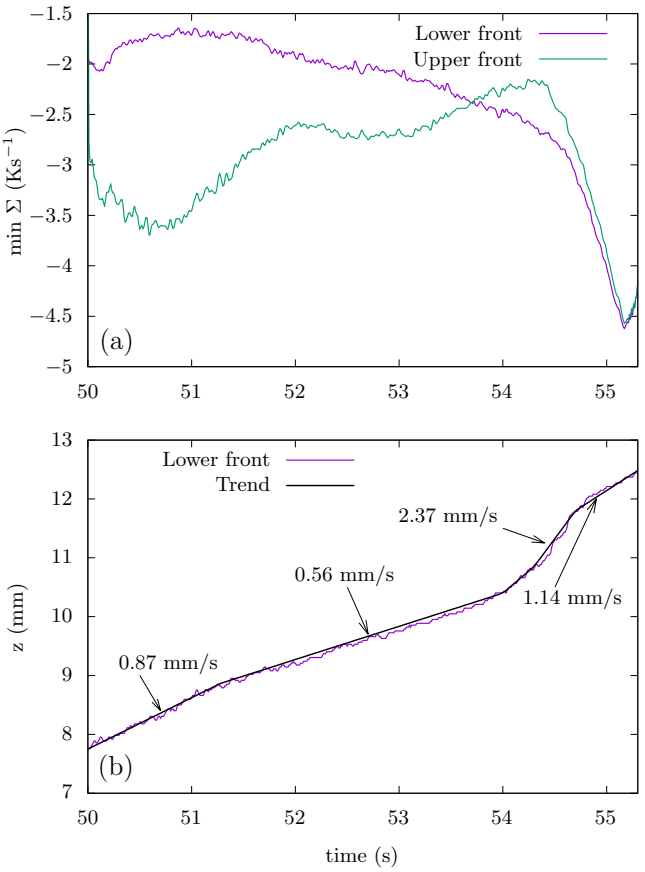

FIG. 5: (a) Minimum of power sink density for each upper and lower front and (b) location of the minimum power sink density points for the lower front as a function of time. Also (b) has been manually adjusted as linear piecewise functions in order to reveal the speed of the lower front in each interval.

These two results confirm, as expected, the intermittent and non-homogeneous behaviour of the transition fronts during their propagation. In order to quantify these changes and make them more visible, for each frame k and for each front (upper and lower), the minimum value of Σ has been determined. To do so, the sample has been divided into two parts: upper part corresponding to $z \in [12.5, 17.5]$ mm and the lower part corresponding to the pixels $z \in [7.5, 12.5)$ mm. The evolution of the minimum value of the heat sink of each front as a function of time has been represented in Fig.5(a). One fact that is observed is the existence of a possible coupling between the dynamics of the fronts. This can be slightly seen in the interval from 50 s to 52 s, and more clearly from 53 s to 54.5 s. If we focus on the interval from 53 s to

54.5 s, as the lower front advances the minimum value of Σ decreases, becoming more negative and thus indicating more cooling power. Contrarily, in the upper front, the minimum value of Σ follows an increasing trend so it shows less cooling power. Just before the fronts merge, the magnitudes of the fronts intersect at $t \approx 53.8$ s.

Also, focusing on the lower front, the spatial coordinate z of the minimum has been recorded. In Fig.5(b) we have represented its position as a function of time. This plot shows explicitly the changes of velocity of the lower front. The graph trend has been manually adjusted as linear piecewise functions. The measured velocities correspond to the slope of each line. After the intersection at $t \approx 53.8$ s, there is a sudden change in the speed of the lower front, from 0.56 mm/s to 2.37 mm/s. Therefore, this result shows that when the lower front accelerates, it starts to cool more.

V. CONCLUSIONS

The study of solid-solid phase transitions is becoming increasingly important in applied physics. One of the big challenges is to understand the dynamics of the heat sinks occurring in structural phase transitions, in order to be able to build environmentally-friendly "cooling" devices. Infrared cameras allow a very fine measurement of the surface temperature, but in order to locate the heat sinks one must reverse Fourier heat equation. Experimental data must be smoothed and it is necessary to use a filtering technique that does not distort the high frequencies, related to the sharp fronts. The results obtained in this work using Gaussian filtering have revealed a better definition and location of the transition fronts than when using uniform averaging. Thus, we have been able to analyze physical variables that give new information about front dynamics. In particular, we have measured the heat sink width, power and velocity. We have revealed details of its non-homogeneous and intermittent dynamics and we have also shown that when several fronts are present its dynamics may show coupling effects.

Acknowledgments

A heartfelt thanks to my advisor Eduard Vives, without his dedication and passion, this work would not have been possible. Many thanks to my parents, my sister and my partner for supporting me at all times. Finally, I would like to dedicate this work to my aunt: wherever you are, thank you for everything.

[1] Otsuka, K., & Wayman, C. M. (Eds.). (1999). *Shape memory materials*. Cambridge University Press.

[2] Bonnot, E., Romero, R., Mañosa, L., Vives, E., & Planes, A. (2008). *Elastocaloric effect associated with the martensitic transition in shape-memory alloys*. Physical Review Letters, 100(12), 125901.

[3] Jani, J. M., Leary, M., Subic, A., & Gibson, M. A. (2014). *A review of shape memory alloy research, applications and opportunities*. Materials & Design (1980-2015), 56, 1078-1113.

[4] Tušek, J., Engelbrecht, K., Millán-Solsona, R., Manosa, L., Vives, E., Mikkelsen, L. P., & Pryds, N. (2015). *The elastocaloric effect: a way to cool efficiently*. Advanced Energy Materials, 5(13), 1500361.

[5] Bhattacharya, K. (2003). *Microstructure of martensite: why it forms and how it gives rise to the shape-memory effect* (Vol. 2). Oxford University Press.

[6] Perez-Reche, F. J., Triguero, C., Zanzotto, G., & Truskinovsky, L. (2016). *Origin of scale-free intermittency in structural first-order phase transitions*. Physical Review B, 94(14), 144102.

[7] Delpueyo, D., Grédiac, M., Balandraud, X., & Badulescu, C. (2012). *Investigation of martensitic microstructures in a monocrystalline Cu–Al–Be shape memory alloy with the grid method and infrared thermography*. Mechanics of Materials, 45, 34-51.

[8] Lebon, G., Jou, D., & Casas-Vázquez, J. (2008). *Understanding non-equilibrium thermodynamics* (Vol. 295). Berlin: Springer.

[9] Delpueyo, D., Balandraud, X., & Grédiac, M. (2013). *Heat source reconstruction from noisy temperature fields using an optimised derivative Gaussian filter*. Infrared Physics & Technology, 60, 312-322.

[10] Ianniciello, L., Romanini, M., Mañosa, L., Planes, A., Engelbrecht, K., & Vives, E. (2020). *Tracking the dynamics of power sources and sinks during the martensitic transformation of a Cu–Al–Ni single crystal*. Applied Physics Letters, 116(18), 183901.

[11] Sauer, T. (2012). *Numerical Analysis*. Pearson